ChemComm

COMMUNICATION

View Article Online
View Journal | View Issue

Cite this: *Chem. Commun.*, 2022, 58, 6829

Received 12th March 2022,
Accepted 4th May 2022

DOI: 10.1039/d2cc01452a

rsc.li/chemcomm

Carbon nano-onion induced organization of polyacrylonitrile-derived block star polymers to obtain mesoporous carbon materials†

Gabriela Siemiaszko, *[a] Agnieszka Hryniewicka,[a] Joanna Breczko, [ab] Krzysztof Brzezinski [c] and Marta E. Plonska-Brzezinska *[a]

Herein, we report the synthesis of mesoporous carbon materials from diblock star copolymers derived from polyacrylonitrile. The size of the pores was controlled by manipulating the length of the polymer blocks. Furthermore, the organization of polymers on the carbon nano-onion's surface resulted in materials of higher surface area and superficial electrochemical performance.

Porous carbon materials are abundantly applied in materials science, especially in electrocatalysis or supercapacitors. Regular pore organization and narrow pore size distribution are crucial for effective porous structures. Carbon materials find different applications depending on the pore size (micro, meso, or macro).[1–4] Targeted morphology can be obtained by applying an appropriate synthetic strategy. One of them is the so-called copolymer soft-templating method involving well-defined copolymers consisting of sacrificial polymer blocks that undergo depolymerization during pyrolysis (*e.g.*, polymethyl acrylate (PMA)) and carbon skeleton-forming polymer blocks, which transform into three-dimensional (3D) networks in the chemical or thermal processes, protecting them from degradation in pyrolysis. The linear copolymers derived from polyacrylonitrile (PAN) are used for the carbon skeleton formation as they form N-doped nanographene due to annealing.[5,6] Polymers of defined length are typically synthesized by controlled radical polymerization methods, including Reversible Addition–Fragmentation Chain Transfer (RAFT) and Atom Transfer Radical (ATR) polymerizations.[7,8]

Porosity and electrochemical performance can be enhanced by incorporating preformed carbon nanostructures into the polymer matrix.[9,10] Carbon nano-onions (CNOs) themselves are attractive materials as electrodes in electric double-layer capacitors (EDLCs) due to their multiple advantages, including high conductivity and thermal stability.[11,12] To the best of our knowledge, the CNO-based nanostructural matrix leading to the organization of PAN-based polymers has not been reported so far. Furthermore, using star-shaped PAN nanostructures to synthesize porous carbon materials is an original approach.

This study reports the preparation of a family of mesoporous carbon materials derived from well-defined star copolymers synthesized using the RAFT radical polymerization method. At first, a series of novel six-arms star copolymers 6-*star*-(polymethyl acrylate-*b*-polyacrylonitrile), (6-*star*-(PMA$_x$-*b*-PAN$_{200}$), x = 25, 50, 100, 150, series from **P1** to **P4**) with an increasing length of PMA chains, were synthesized (Fig. 1A). Their structure was confirmed by Nuclear Magnetic Resonance Spectroscopy (^{1}H NMR) and Fourier Transform Infrared Spectroscopy (FTIR) (Fig. S1–S4 and S5a–d, ESI†). Size-exclusion chromatography (SEC) confirmed synthesis a series of star polymers with growing molecular masses ($M_{n,SEC}$) in the range from 87 000 to 127 000 g mol^{-1} (Fig. 1B and Fig. S6, ESI†) similar to those estimated theoretically and by ^{1}H NMR (Table S1, ESI†). The mass fraction of PMA chains (wt% PMA) in the molecules was determined based on the integration of the –CH$_3$ signal of ester groups and the proton adjacent to nitrile (–CHCN) in the ^{1}H NMR spectra, proving the increase of this value from 15 to 55% in the series from **P1** to **P4**. The wt% PMA and the $M_{n,SEC}$ values were used to estimate the molecular masses of PMA in polymers ($M_{n,PMA}$). The polymers were then subjected to annealing for 4 h at 250 °C under airflow to stabilize PAN domains, providing products from **P1-S** to **P4-S**. Subsequent pyrolysis for 2 h at 800 °C under an Ar atmosphere afforded carbon samples from **P1-C** to **P4-C**. The weight loss of the

[a] *Department of Organic Chemistry, Faculty of Pharmacy with the Division of Laboratory Medicine, Medical University of Bialystok, Mickiewicza 2A, 15-222 Bialystok, Poland. E-mail: gsiemiaszko@gmail.com, marta.plonska-brzezinska@umb.edu.pl*

[b] *Faculty of Chemistry, University of Bialystok, Ciolkowskiego 1K, 15-245 Bialystok, Poland*

[c] *Department of Structural Biology of Prokaryotic Organisms, Institute of Bioorganic Chemistry, Polish Academy of Sciences, Noskowskiego 12/14, 61-074, Poznan, Poland*

† Electronic supplementary information (ESI) available. See DOI: https://doi.org/10.1039/d2cc01452a

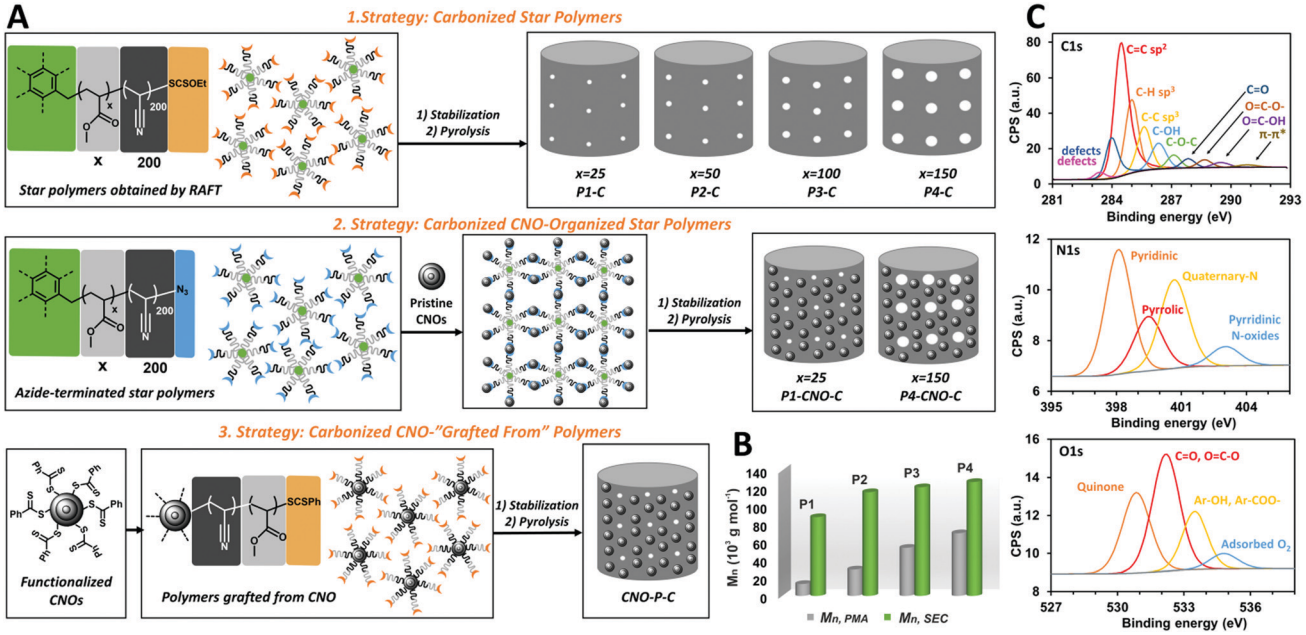

Fig. 1 (A) Schematic representation of the synthesis steps of carbonaceous materials. Three different strategies have been used to synthesize of porous materials; please see ESI.† (B) Molecular masses of **P1-P4** polymers determined by SEC. (C) XPS spectra of **P4-CNO-C** C 1s, N 1s, and O 1s spectral regions. The C 1s, O 1s, and N 1s high-resolution spectra were recorded at pass energy of 50 eV at room temperature.

samples during thermal treatment increased in direct proportion to the PMA content indicating pores forming in the carbon materials (Table S2, ESI†). FTIR measurements confirmed both thermal steps.

The characteristic signals of ester groups, C═O (1730 cm^{-1}), C–O (1150 cm^{-1}) and nitriles (2240 cm^{-1}) disappeared due to PMA depolymerization or cross-linking and cyclization reaction of –CN, respectively, resulting in C═C (1587 cm^{-1}) and C–N (1363 cm^{-1}) bonds formation (Fig. S5e and f, ESI†).[13]

Afterward, we attempted to hierarchically organize selected polymeric stars **P1** and **P4** on the CNO's surface (Fig. 1A). For this purpose, dithiocarbonate groups (–SCSOEt) at the ends of polymeric stars' arms were transformed into azide groups ($–N_3$), confirmed by the disappearance of $–CH_2–$ at *ca.* 4.60 ppm on the ^{1}H NMR spectra (Fig. S7 and S8, ESI†). The products were subjected to reactions with CNOs to generate aziridine linkages between polymers and carbon nanoparticles.[14] FTIR analysis supports that the resulting polymer-carbon hybrids possessed characteristic polymer (C═O and CN) signals on the CNO's surface (Fig. S5g and h, ESI†). Next, **P1-CNO** and **P4-CNO** were stabilized and pyrolyzed using general procedures to give carbon materials: **P1CNO-C** and **P4-CNO-C**. CNOs content of *ca.* 5–6% was estimated by dividing the mass of CNOs used in the synthesis by the weight of the pyrolyzed hybrid sample (Table S2, ESI†).

Another approach to the CNO-induced 3D organization of polyacrylonitrile-derived block polymers was based on the formation of polymeric chains grafted from carbon nanostructures (Fig. 1A). For this purpose, the CNO-derived chain transfer agent dithiocarbonate (**CNO-SCSPh**) was used to carry out controlled polymerization of acrylonitrile and methyl acrylate consecutively, affording carbon nanoparticles decorated with PAN-*b*-PMA copolymers (**CNO-P**). The course of the synthetic steps was followed by FTIR analysis, proving the growth of the polymeric chains on the CNO's surface supported by increasing intensity of characteristic signals of CN, C═O, C–C (1430 cm^{-1}), and C–O groups (Fig. S5i–k, ESI†). As a result of annealing, the **CNO-P-C** carbon material was obtained with a CNO's content of *ca.* 2% (Table S2, ESI†).

X-ray Photoelectron Spectroscopy (XPS) was applied to determine the elemental composition of the surface of the **C1-C**, **C4-C**, **C1-CNO-C**, **C4-CNO-C**, and **CNO-P-C** materials. The results indicate the presence of C (84–90%), N (4–8%), and O (4–9%) in all studied materials (Table S3, ESI†). The deconvolution of the high-resolution spectral regions C 1s, O 1s, and N 1s of **C4-CNO-C** indicate a pattern of distribution of elements (Fig. 1C). Carbon atom forms mainly C═C sp^2, C–H sp^3, and C–C sp^3 bonds.

Bonding with oxygen results in the presence of C–OH, C–O–C, C═O, O═C–O, and O═C–OH groups.[15,16] Furthermore, the sample is characterized by defects in carbon structure and π–π* interactions.[17,18] The N 1s spectrum can be resolved into four regions indicating the formation of mainly pyridinic and quaternary N, as well as pyrrolic and *N*-pyridinic oxides to a smaller extent.[19,20] The O 1s analysis supports the content of dominantly C═O, O═C–O, quinone, Ar–OH, and Ar–COO– moieties.[21] The remaining analyzed samples have a very similar elemental distribution pattern (Table S4 and Fig. S9, ESI†). Except for the quinone to Ar–OH/Ar–COO– ratio, which is dependent on the quinone–quinol equilibrium.[22] These functional groups are beneficial for surface redox reactions related to the material's pseudocapacitance.

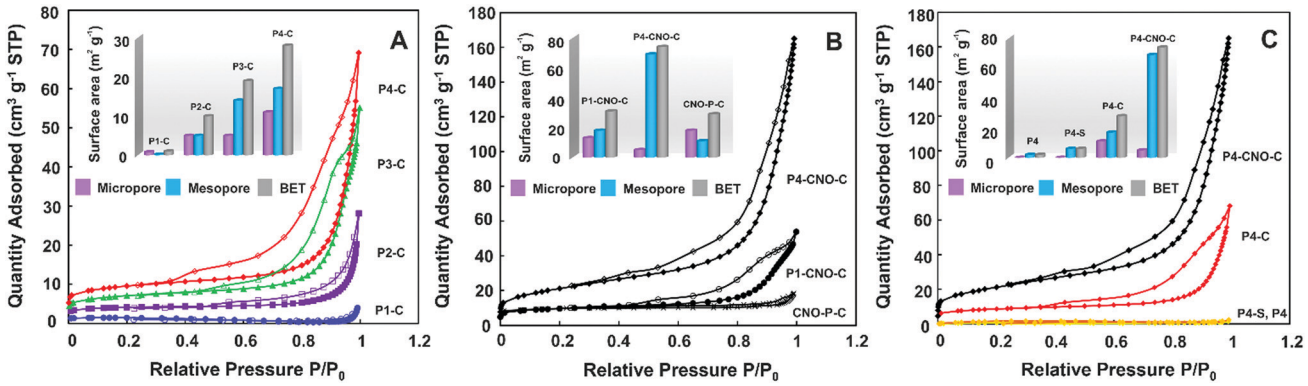

Fig. 2 Nitrogen adsorption/desorption isotherms of (A) **P1-C**, **P2-C**, **P3-C**, **P4-C**, (B) **CNO-P-C**, **P1-CNO-C**, **P4-CNO-C**, and (C) **P4**, **P4-S**, **P4-C**, and **P4-CNO-C**. Insert: BET surface area values and contribution of micropores and mesopores in the surface of analyzed materials.

The study of the porosity of pyrolyzed 6-*star*-(PMA$_x$-*b*-PAN$_{200}$) polymers (Fig. 2A) clearly showed the significant influence of the PMA chain length on the amount of N_2 adsorbed on the material's surface. Namely, the longer the polymer chain, the higher the quantity of adsorbed gas observed, which corresponds to the greater specific surface area (S_{BET}) of the studied materials.

The presence of CNOs in the **P1-CNO-C**, **P4-CNO-C**, and **CNO-P-C** structures also resulted in significant growth in the porosity (Fig. 2B) compared to the corresponding pristine polymers. The course of all recorded curves (Fig. 2) was a combination of type I and IV isotherms, indicating the coexistence of micro- and mesopores in the structure of the pyrolyzed carbon materials.[23] Analysis of isotherms based on the Brunauer–Emmett–Teller (BET) theory,[24] allowed us to determine S_{BET} values (insert of Fig. 2, Fig. S10 and Table S5, ESI†), which increased linearly with an increase of the length of the polymeric chain (Fig. 2A and B and Table S5, ESI†). The *t*-plot analysis demonstrated that a significant part of the S_{BET} values calculated for the studied materials derives from mesopores (Table S5, ESI†). However, it is of note that the increase in the surface area of mesopores is more distinct for the longer polymeric chains (**P4-C**) (insert of Fig. 2A and Table S5, ESI†). Although the same tendency is also apparent for materials containing the CNOs, the difference between the surface area of micro- and mesopores is even more pronounced for **P1-CNO-C** and **P4-CNO-C** (insert of Fig. 2B and Table S5, ESI†). The successive increase in the pore diameter controlled at each synthesis step is shown in Fig. 2C. The graph confirms the growth in the surface area of mesopores due to the stabilization and pyrolysis processes in the presence of CNOs.

The morphology of all the pyrolyzed star 6-*star*-(PMA-*b*-PAN) polymers (from **P1-C** to **P4-C**) and those containing the CNOs (**P1-CNO-C**, **P4-CNO-C**, **CNO-P-C**) was studied using scanning electron microscopy (SEM) (Fig. 3). The images obtained for **P1-C** and **P4-C** (Fig. 3A and B, respectively) show that copolymers form a granular morphology with a different diameter of the aggregates. The copolymers with the shorter polymeric chains tend to aggregate with various sizes, while the longer ones form aggregates with approx. 1–2 μm (Fig. S11, ESI†). The

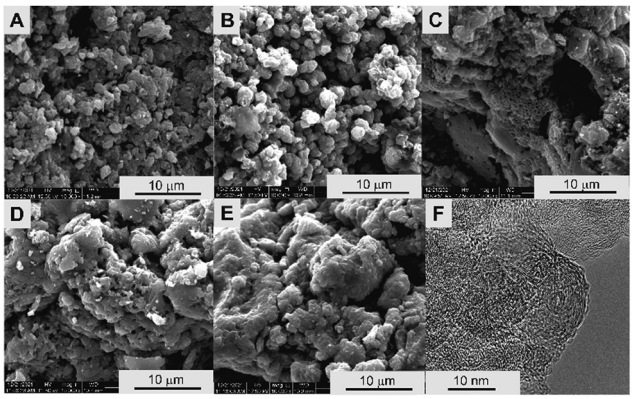

Fig. 3 SEM images of (A) **P1-C**, (B) **P4-C**, (C) **CNO-P-C**, (D) **P1-CNO-C**, and (E) **P4-CNO-C**. (F) HRTEM image of **P4-CNO-C**.

structure of the carbon materials containing CNOs (Fig. 3C–E and Fig. S12, ESI†) appears more spongy and 3D than the pyrolyzed pristine polymers (Fig. 3A and B), indicating an increase in the number of channels and cavities, and thus the porosity enhancement. These observations agree with experimental data obtained by the N_2 adsorption/desorption method. SEM observations are carried out at the microscale level, while the pores are only visible at the nano-level. Therefore, high-resolution transmission electron microscopic (HRTEM) studies were performed to analyze the carbonaceous materials (Fig. 3F and Fig. S13, ESI†). All samples derived from copolymers and CNOs have uniformly distributed spherical cavities in the structure, which may be assigned to pores (Fig. S13b, ESI†). The addition of CNOs to the polymeric materials causes an increase in crystallinity. These studies of the materials containing CNOs (**P4-CNO-C**) clearly show the presence of multilayered fullerenes in their structure.

These observations are also confirmed by X-ray diffraction study (XRD). For all materials, the most substantial asymmetric peak located around the 2θ angle between 22–25° corresponds to the graphite's (002) plane,[23,24] that suggests the presence of sp^2-bonded carbon atoms (Fig. S15, ESI†). The addition of CNOs to the polymer sample increases the crystallinity of these

hybrid materials. The (002) reflection is sharper for **P1-CNO-C** and **P4-CNO-C** materials compared to polymer reference samples (**P1-C** and **P4-C**), suggesting that the materials containing CNO's moiety are the graphite-like structures with a higher-order spacial arrangement (additional information please see ESI†).

The electrochemical performance of all synthesized samples was investigated (Fig. S16–S18, ESI†). Considering that cyclic voltammetry (CV) allows us to easily show the relationship between the S_{BET} and the specific capacitance (C_S), we made measurements in a three-electrode system with the 1 M NaOH aqueous solution as a supporting electrolyte. The CVs recorded for the GCE electrode modified with the synthesized materials have an approximately rectangular shape, thus showing an EDL capacitor behavior. As expected, the obtained C_S values were more significant, the higher the porosity and the longer the PMA chains in the structure of the tested material (Fig. S16 and Table S6, ESI†). The use of CNOs for the organization of the polymer network also contributed to a significant increase in the double layer capacitance (Fig. S17 and Table S6, ESI†). For shorter polymer chains (**P1-C**), the addition of CNOs to the polymer matrix (**P1-CNO-C**) causes a tenfold increase in the C_S values, from 5 to 83 F g^{-1}, respectively. As the length of the polymer chain increases, so does the value of the C_S also increases. The **P4-CNO-C** (C_S = 83 F g^{-1}) exhibited the highest electrochemical capacitance. These observations agree with experimental data obtained by the N_2 adsorption/desorption method. For this material, the largest pore volume of 0.2364 cm^3 g^{-1} was also noted, with the majority in the micropore area (diameter below 2 nm) and in the mesopore area (diameter in the range of 8–20 nm) (Fig. S10, ESI†).

Electrochemical stability of **P4-CNO-C** in the wide potential range was also performed (Fig. S18, ESI†). Despite the functional groups containing N and O occurring in all materials, a contribution from a possible pseudocapacitance (faradaic reactions) is not detected in the CV curves in the studied potential window. Such observations have already been made in previous literature reports for porous carbon materials.[25]

In this study, we demonstrated the organization of star copolymers (6-*star*-(PMA-*b*-PAN)) on the CNO's surface, giving well-organized 3D porous structures with mesoporous characteristics. The selection of the appropriate polymerization method for the nanostructured matrix and the length of the polymer chain allowed us to synthesize a material with a homogeneous mesopore arrangement. The textural properties of this material, along with its high conductivity, make it possible to use it as an electrode material in supercapacitors and in the future in electrocatalysis.

We gratefully acknowledge the financial support of the National Science Centre, Poland, grant #2017/25/B/ST5/01414 to M.E.P-B. We gratefully acknowledge Prof. Luis Echegoyen from University of Texas at El Paso for providing the CNOs. Prof. Jacek Gebicki (Gdańsk University of Technology, Poland) is acknowledged for performing SEC analysis. The research was carried out with the equipment purchased thanks to the financial support of the European Regional Development Fund in the framework of the Polish Innovation Economy Operational Program (POIG.02.01.00-06024/09, Maria Curie-Sklodowska University, Lublin, Poland) and the Operational Program Development of Eastern Poland 2007–2013 (POPW.01.03.00-20-034/09-00 and POPW.01.03.00-20-004/11, University of Bialystok, Poland).

Conflicts of interest

There are no conflicts to declare.

References

1 C. Xie, D. Yan, H. Li, S. Du, W. Chen, Y. Wang, Y. Zou, R. Chen and S. Wang, *ACS Catal.*, 2020, **10**, 11082–11098.
2 M. R. Benzigar, S. N. Talapaneni, S. Joseph, K. Ramadass, G. Singh, J. Scaranto, U. Ravon, K. Al-Bahily and A. Vinu, *Chem. Soc. Rev.*, 2018, **47**, 2680–2721.
3 Q. Huang, Y. Xu, Y. Guo, L. Zhang, Y. Hu, J. Qian and S. Huang, *Carbon*, 2022, **188**, 135–145.
4 Q. Huang, Y. Guo, D. Chen, L. Zhang, T.-T. Li, Y. Hu, J. Qian and S. Huang, *Chem. Eng. J.*, 2021, **424**, 130336.
5 J. P. McGann, M. Zhong, E. K. Kim, S. Natesakhawat, M. Jaroniec, J. F. Whitacre, K. Matyjaszewski and T. Kowalewski, *Macromol. Chem. Phys.*, 2012, **213**, 1078–1090.
6 M. Kopeć, M. Lamson, R. Yuan, C. Tang, M. Kruk, M. Zhong, K. Matyjaszewski and T. Kowalewski, *Prog. Polym. Sci.*, 2019, **92**, 89–134.
7 Z. Zhou, T. Liu, A. U. Khan and G. Liu, *Sci. Adv.*, 2019, **5**, eaau6852.
8 M. Kopeć, R. Yuan, E. Gottlieb, C. M.-R. Abreu, Y. Song, Z. Wang, J. F.-J. Coelho, K. Matyjaszewski and T. Kowalewski, *Macromolecules*, 2017, **50**, 2759–2767.
9 A. Cymann-Sachajdak, M. Graczyk-Zajac, G. Trykowski and M. Wilamowska-Zawłocka, *Electrochim. Acta*, 2021, **383**, 138356.
10 M. Suleman, M. Deraman, S. A. Hashmi, M. A.-R. Othman, Y. Kumar, S. K. Rajouria and M. R.-M. Jasni, *Electrochim. Acta*, 2020, **333**, 135547.
11 M. E. Plonska-Brzezinska and L. Echegoyen, *J. Mater. Chem. A*, 2013, **1**, 13703.
12 O. Mykhailiv, A. Lapinski, A. Molina-Ontoria, E. Regulska, L. Echegoyen, A. T. Dubis and M. E. Plonska-Brzezinska, *Chem. Phys. Chem.*, 2015, **16**, 2182–2191.
13 C. Tang, K. Qi, K. L. Wooley, K. Matyjaszewski and T. Kowalewski, *Angew. Chem., Int. Ed.*, 2004, **43**, 2783–2787.
14 J. Han and C. Gao, *Nano-Micro Lett.*, 2010, **2**, 213–226.
15 M. Koinuma, H. Tateishi, K. Hatakeyama, S. Miyamoto, C. Ogata, A. Funatsu, T. Taniguchi and Y. Matsumoto, *Chem. Lett.*, 2013, **42**, 924–926.
16 G. Radaelli, J. A. Heredia-Guerrero, M. T. Masood, L. Ceseracciu, A. Davis, R. Carzino, M. Prato, I. S. Bayer and A. Athanassiou, *Adv. Mater. Interfaces*, 2016, **3**, 1600069.
17 H. Xu, B. Yang, J. Wang, S. Guang and C. Li, *Macromolecules*, 2005, **38**, 10455–10460.
18 Y.-C. Chiang, Y.-J. Chen and C.-Y. Wu, *Materials*, 2017, **10**, 1296.
19 R. Arrigo, M. Hävecker, S. Wrabetz, R. Blume, M. Lerch, J. McGregor, E. P.-J. Parrott, J. A. Zeitler, L. F. Gladden, A. Knop-Gericke, R. Schlögl and D. S. Su, *J. Am. Chem. Soc.*, 2010, **132**, 9616–9630.
20 S. K. Ujjain, R. Bhatia and P. Ahuja, *J. Saudi Chem. Soc.*, 2019, **23**, 655–665.
21 Y. J. Oh, J. J. Yoo, Y. I. Kim, J. K. Yoon, H. N. Yoon, J.-H. Kim and S. B. Park, *Electrochim. Acta*, 2014, **116**, 118–128.
22 H. Berg and P. Zuman, *J. Chem. Soc., Perkin Trans. 2*, 2000, 1459–1464.
23 K. S.-W. Sing, *Pure Appl. Chem.*, 1982, **54**, 2201–2218.
24 S. Brunauer, P. H. Emmett and E. Teller, *J. Am. Chem. Soc.*, 1938, **60**, 309–319.
25 J. Chen, Y. Han, X. Kong, X. Deng, H. J. Park, Y. Guo, S. Jin, Z. Qi, Z. Lee, Z. Qiao, R. S. Ruoff and H. Ji, *Angew. Chem., Int. Ed.*, 2016, **55**, 13822–13827.

